

Driven Tunneling: Chaos and Decoherence

Peter Hänggi¹, Sigmund Kohler², and Thomas Dittrich³

¹ Institut für Physik, Universität Augsburg, D-86135 Augsburg, Germany

² Depto. de Física Teórica de la Materia Condensada, Universidad Autónoma, E-28049 Madrid, Spain

³ Depto. de Física, Universidad de los Andes, Santafé de Bogotá, Colombia

Abstract. Chaotic tunneling in a driven double-well system is investigated in absence as well as in the presence of dissipation. As the constitutive mechanism of chaos-assisted tunneling, we focus on the dynamics in the vicinity of three-level crossings in the quasienergy spectrum. They are formed when a tunnel doublet, located on a pair of symmetry-related tori in the classical phase space, approaches a chaotic singlet in energy. The coherent quantum dynamics near the crossing, in particular the enhanced tunneling that involves the chaotic singlet state as a “step stone”, is described satisfactorily by a three-state model. It fails, however, for the corresponding dissipative dynamics, because incoherent transitions due to the interaction with the environment indirectly couple the three states in the crossing to the remaining quasienergy states. We model dissipation by coupling the double well, the driving included, to a heat bath. The time dependence of the central system, with a quasienergy spectrum containing exponentially small tunnel splittings, requires special considerations when applying the Born-Markov and rotating-wave approximations to derive a master equation for the density operator. We discuss the effect of decoherence on the now transient chaos-assisted tunneling: While decoherence is accelerated practically independent of temperature near the center of the crossing, it can be stabilized with increasing temperature at a chaotic-state induced exact crossing of the ground-state quasienergies. Moreover the asymptotic amount of coherence left within the vicinity of the crossing is enhanced if the temperature is below the splitting of the avoided crossing; but becomes diminished when temperature raises above the splitting (chaos-induced coherence or incoherence, respectively). The asymptotic state of the driven dissipative quantum dynamics partially resembles the, possibly strange, attractor of the corresponding damped driven classical dynamics, but also exhibits characteristic quantum effects.

1 Introduction

The interplay of classical chaos and dissipation in a quantum system bears interesting effects at the border between classical and quantum mechanics like, e.g., the suppression of classical chaos by quantum interference [1] or its restauration by dissipation [2]. While the mutual influence of quantum coherence and classical chaos is under investigation since many years, the additional effects caused by coupling the chaotic system to an environment, namely dissipation and decoherence, have been studied only rarely. One reason is that by including dissipation, the computational effort grows drastically, since one has to deal with density matrices instead of wave functions.

In classical Hamiltonian systems, the transition from regular motion to chaos is most clearly visible in the change of the phase-space structure: With increasing nonlinearity, regular tori successively dissolve in adjacent chaotic layers which grow in size and merge until the whole phase space is uniformly covered by a chaotic sea where the dynamics is locally hyperbolic and globally diffusive [3]. Research in quantum chaos has initially been concentrated on this limiting case of “hard chaos”, because the absence of structure in phase space facilitates the description.

Closer to the generic situation, however, is the intermediate regime with an extremely intricate interweaving of regular and chaotic areas, as described by the Kolmogorov-Arnol’d-Moser (KAM) theorem, with self-similar hierarchies of regular islands. It is in this regime that we expect the most interesting, but at the same time least tractable, phenomena of chaos-coherence interplay to occur. A prominent example is chaotic tunneling, the coherent exchange of probability between symmetry-related regular regions that are separated dynamically by a chaotic layer, instead of a static potential barrier [4–20]. Chaotic tunneling comes about by the simultaneous action of classical nonlinear dynamics and quantum coherence. Tunneling is extremely sensitive to any disruption of coherence as it occurs due to the unavoidable coupling to the environment: In presence of dissipation, coherent tunneling becomes a transient that fades out on the way to an asymptotic state [21, 22]. This is just one instance of the general rule that decoherence tends to restore classical behaviour, other examples being the partial lifting, by dissipation, of the quantum suppression of chaos, and the appearance of quantum stationary states that show a close resemblance to corresponding classical strange attractors [2]. However, particularly for weak dissipation, more complicated cross effects occur, such as the strong modification of the decoherence time by chaotic tunneling.

In this contribution, we investigate the mutual influence of chaotic tunneling and dissipation for a specific, but nevertheless generic case: a periodically forced bistable system. The quartic double well with a harmonic driving will serve as our working model. In Section 2 we introduce its Hamiltonian and the underlying symmetries. To provide the necessary background, we also briefly review other important features of this system, in particular driven tunneling and its coherent suppression and modification in the presence of classical chaos without damping.

Dealing with a driven system, its quantum dynamics is adequately analyzed in terms of the Floquet or quasienergy spectrum, also introduced in Section 2. The quasispectrum associated with chaotic tunneling exhibits a characteristic feature: Quasienergies of chaotic singlets frequently intersect tunnel doublets which are supported by regular tori. As the basic mechanism of chaotic tunneling we study, in Sections 3 and 4, the coherent and dissipative quantum dynamics in the vicinity of such singlet-doublet crossings. While in the coherent case the dynamics is well described in a three-state approximation, the coupling to the environment indirectly couples the three states to all other states. On the basis of numerical results for the full driven double well with dissipation, we reveal the limitations of the three-level approximation and identify additional features

of the full dynamics not covered by it. In particular, we consider the long-time asymptotics and the phase-space structure associated with it.

Also on the classical level, the presence of friction has profound consequences for the phase-space structure: Due to the net contraction of phase-space volume, stationary states are restricted to manifolds of lower dimensionality than the underlying phase space. Depending on friction strength and details of the system, this attractor may consist of fixed points, of limit cycles, or, if the classical dynamics is chaotic, of a strange attractor with self-similar, fractal geometry. On a quantum level, the structures associated with classical attractors are smeared out on a scale \hbar , yet leave clear traces in the asymptotic state of the corresponding dissipative quantum dynamics [23]. We study the classical-quantum correspondence of the asymptotic state in Section 5.

2 The model

We consider the quartic double well with a spatially homogeneous driving force, harmonic in time. It is defined by the Hamiltonian

$$H(t) = H_{\text{DW}} + H_F(t), \quad (1)$$

$$H_{\text{DW}} = \frac{p^2}{2m} - \frac{1}{4}m\omega_0^2x^2 + \frac{m^2\omega_0^4}{64E_B}x^4, \quad (2)$$

$$H_F(t) = Sx \cos(\Omega t). \quad (3)$$

The potential term of the static bistable Hamiltonian H_{DW} possesses two minima at $x = \pm x_0$, $x_0 = (8E_B/m\omega_0^2)^{1/2}$, separated by a barrier of height E_B (cf. Fig. 1). The parameter ω_0 denotes the (angular) frequency of small oscillations near the bottom of each well. Apart from mere scaling, the classical phase space of H_{DW} only depends on the presence or absence, and the signs, of the x^2 and the x^4 term. Besides that, it has no free parameter. This is obvious from the scaled form of the classical equations of motion,

$$\dot{\bar{x}} = \bar{p}, \quad (4)$$

$$\dot{\bar{p}} = \frac{1}{2}\bar{x} - \frac{1}{2}\bar{x}^3 - F \cos(\bar{\Omega}\bar{t}), \quad (5)$$

where the dimensionless quantities \bar{x} , \bar{p} and \bar{t} are given by x/x_0 , $p/m\omega_0x_0$ and ω_0t , respectively. The influence of the driving on the classical phase-space structure is fully characterized by the rescaled amplitude and frequency of the driving,

$$F = \frac{S}{\sqrt{8m\omega_0^2E_B}}, \quad \bar{\Omega} = \frac{\Omega}{\omega_0}. \quad (6)$$

This implies that the classical dynamics is independent of the barrier height E_B .

In the quantum-mechanical case, this is no longer true: The finite size of Planck's constant results in a finite number

$$D = \frac{E_B}{\hbar\omega_0} \quad (7)$$

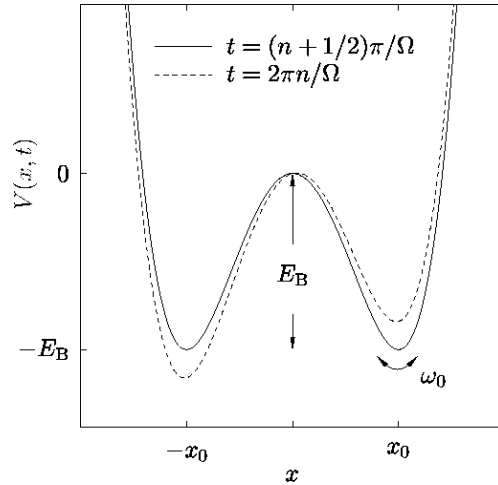


Fig. 1. Sketch of the driven double well potential described by the time-dependent Hamiltonian (1) at two different phases.

of doublets with energy below the barrier top. The classical limit amounts to $D \rightarrow \infty$. This is evident from the classical scales for position, x_0 , and momentum, $m\omega_0 x_0$, introduced above: The corresponding action scale is $m\omega_0 x_0^2$ and therefore, the position-momentum uncertainty relation in the scaled phase space (\bar{x}, \bar{p}) reads

$$\Delta\bar{x} \Delta\bar{p} \geq \frac{\hbar_{\text{eff}}}{2}, \quad (8)$$

where

$$\hbar_{\text{eff}} = \frac{\hbar}{m\omega_0 x_0^2} = \frac{1}{8D} \quad (9)$$

denotes the effective quantum of action.

In the following, we restrict the driving amplitude to moderate values, such that the difference between the potential minima remains much smaller than the barrier height. This implies that the bistable character of the potential is never lost.

2.1 Symmetries

Time periodicity. The Hamiltonian (1) is P -periodic, with $P = 2\pi/\Omega$. As a consequence of this discrete time-translational invariance of $H(x, p; t)$, the relevant generator of the quantum dynamics is the Floquet operator [24–28]

$$U = \mathcal{T} \exp \left(-\frac{i}{\hbar} \int_0^P dt H(t) \right), \quad (10)$$

where \mathcal{T} denotes time ordering. According to the Floquet theorem, the adiabatic states of the system are the eigenstates of U . They can be written in the form

$$|\psi_\alpha(t)\rangle = e^{-i\epsilon_\alpha t/\hbar} |\phi_\alpha(t)\rangle, \quad (11)$$

with

$$|\phi_\alpha(t + P)\rangle = |\phi_\alpha(t)\rangle.$$

Expanded in these Floquet states, the propagator of the driven system reads

$$U(t', t) = \sum_\alpha e^{-i\epsilon_\alpha(t'-t)/\hbar} |\phi_\alpha(t')\rangle \langle \phi_\alpha(t)|. \quad (12)$$

The associated eigenphases ϵ_α , referred to as quasienergies, come in classes, $\epsilon_{\alpha,n} = \epsilon_\alpha + n\hbar\Omega$, $n = 0, \pm 1, \pm 2, \dots$. This is suggested by a Fourier expansion of the $|\phi_\alpha(t)\rangle$,

$$\begin{aligned} |\phi_\alpha(t)\rangle &= \sum_n |c_{\alpha,n}\rangle e^{-in\Omega t}, \\ |c_{\alpha,n}\rangle &= \frac{1}{P} \int_0^P dt |\phi_\alpha(t)\rangle e^{in\Omega t}. \end{aligned} \quad (13)$$

The index n counts the number of quanta in the driving field. Otherwise, the members of a class α are physically equivalent. Therefore, the quasienergy spectrum can be reduced to a single ‘‘Brillouin zone’’, $-\hbar\Omega/2 \leq \epsilon < \hbar\Omega/2$.

Since the quasienergies have the character of phases, they can be ordered only locally, not globally. A quantity that is defined on the full real axis and therefore does allow for a complete ordering, is the mean energy [22, 27, 28]

$$E_\alpha = \frac{1}{P} \int_0^P dt \langle \psi_\alpha(t) | H(t) | \psi_\alpha(t) \rangle \equiv \langle \langle \phi_\alpha(t) | H(t) | \phi_\alpha(t) \rangle \rangle. \quad (14)$$

It is related to the corresponding quasienergy by

$$E_\alpha = \epsilon_\alpha + \langle \langle \phi_\alpha(t) | i\hbar \frac{\partial}{\partial t} | \phi_\alpha(t) \rangle \rangle, \quad (15)$$

where the outer angle brackets denote the time average over one period of the driving, as indicated by Eq. (14). The second term on the right-hand side plays the rôle of a geometric phase accumulated over this period [22, 29]. Without the driving, $E_\alpha = \epsilon_\alpha$, as it should be. By inserting the Fourier expansion (13), the mean energy takes the form

$$E_\alpha = \sum_n (\epsilon_\alpha + n\hbar\Omega) \langle c_{\alpha,n} | c_{\alpha,n} \rangle. \quad (16)$$

It shows that the n th Floquet channel gives a contribution $\epsilon_\alpha + n\hbar\Omega$ to the mean energy, weighted by the Fourier coefficient $\langle c_{\alpha,n} | c_{\alpha,n} \rangle$ [28].

Quasienergies and Floquet states are obtained numerically by solving the matrix eigenvalue equation [24, 27, 28]

$$\sum_{n'} \sum_{k'} \mathcal{H}_{n,k;n',k'} c_{n',k'} = \epsilon c_{n,k}, \quad (17)$$

equivalent to the time-dependent Schrödinger equation. It is derived by inserting the eigenstates (11) into the Schrödinger equation, Fourier expanding, and using the representation in the eigenbasis of the unperturbed Hamiltonian, $H_0|\Psi_k\rangle = E_k|\Psi_k\rangle$. We introduced the abbreviations

$$\mathcal{H}_{n,k;n',k'} = (E_k - n\hbar\Omega)\delta_{n-n'}\delta_{k-k'} + \frac{1}{2}S_{x_{k,k'}}(\delta_{n-1-n'} + \delta_{n+1-n'}), \quad (18)$$

$$c_{n,k} = \langle\Psi_k|c_n\rangle, \quad (19)$$

$$x_{k,k'} = \langle\Psi_k|x|\Psi_{k'}\rangle. \quad (20)$$

Time-reversal symmetry. The energy eigenfunctions of an autonomous Hamiltonian with time-reversal symmetry,

$$\mathbb{T} : \quad x \rightarrow x, \quad p \rightarrow -p, \quad t \rightarrow -t \quad (21)$$

can be chosen as real [30, 31]. Time-reversal invariance is generally broken by a magnetic field or by an explicit time-dependence of the Hamiltonian. However, for the sinusoidal shape of the driving together with the initial phase chosen above, \mathbb{T} invariance is retained and the Schrödinger operator $\mathcal{H}(t) = H(t) - i\hbar\partial_t$ obeys $\mathcal{H}(t) = \mathcal{H}^*(-t)$. If now $\phi(x, t)$ is a Floquet state in position representation with quasienergy ϵ , then $\phi^*(x, -t)$ also is a Floquet state with the same quasienergy. This means that we can always find a linear combination of these Floquet states such that $\phi(x, t) = \phi^*(x, -t)$, or in the frequency domain, $\phi(x, \Omega) = \phi^*(x, \Omega)$, i.e., the Fourier coefficients of the Floquet states can be chosen real.

Generalized parity. The invariance of H_{DW} under parity $\mathbb{P} : x \rightarrow -x, p \rightarrow -p, t \rightarrow t$ is destroyed by any spatially constant driving force. With the above choice of $H_F(t)$, however, a more general, dynamical symmetry remains [32–34]. It is defined by the operation

$$\mathbb{P}_P : \quad x \rightarrow -x, \quad p \rightarrow -p, \quad t \rightarrow t + P/2 \quad (22)$$

and represents a generalized parity acting in the extended phase space spanned by x, p , and phase, i.e., time $t \bmod P$. While such a discrete symmetry is of minor importance in classical physics, its influence on the quantum mechanical quasispectrum $\{\epsilon_\alpha(F)\}$ is profound: It divides the Hilbert space in an even and an odd sector, thus allowing for a classification of the Floquet states as even or odd. Quasienergies from different symmetry classes may intersect, while quasienergies with the same symmetry typically form avoided crossings [31]. The fact that \mathbb{P}_P acts in the phase space extended by time $t \bmod P$, results in a particularity: If, e.g., $|\phi(t)\rangle$ is an even Floquet state, then $\exp(i\Omega t)|\phi(t)\rangle$ is odd, and vice versa. Thus, two equivalent Floquet states from neighboring Brillouin zones have opposite generalized parity. This means that a classification of the corresponding solutions of the Schrödinger equation, $|\psi(t)\rangle = \exp(-iet/\hbar)|\phi(t)\rangle$, as even or odd is meaningful only with respect to a given Brillouin zone.

The invariance of the system under P_P is also of considerable help in the numerical treatment of the Floquet matrix (18) [11, 12]. To obtain a complete set of Floquet states, it is sufficient to compute all eigenvectors of the Floquet Hamiltonian in the even subspace whose eigenvalues lie in the first two Brillouin zones. The even Floquet states are given by the eigenvectors of \mathcal{H}_e from the first Brillouin zone; the odd Floquet states are obtained by shifting the (even) ones from the second to the first Brillouin zone, which changes their generalized parity. Thus, in the even subspace, we have to diagonalize the matrix

$$\mathcal{H}_e = \begin{pmatrix} \ddots & \vdots & \vdots & \vdots & \vdots & \vdots & \vdots & \vdots \\ \cdots & E_e + 2\hbar\Omega & X_{eo} & 0 & 0 & 0 & \cdots & \cdots \\ \cdots & X_{eo} & E_o + \hbar\Omega & X_{oe} & 0 & 0 & \cdots & \cdots \\ \cdots & 0 & X_{oe} & E_e & X_{eo} & 0 & \cdots & \cdots \\ \cdots & 0 & 0 & X_{eo} & E_o - \hbar\Omega & X_{oe} & \cdots & \cdots \\ \cdots & 0 & 0 & 0 & X_{oe} & E_e - 2\hbar\Omega & \cdots & \cdots \\ \vdots & \vdots & \vdots & \vdots & \vdots & \vdots & \vdots & \ddots \end{pmatrix}. \quad (23)$$

For the same number of Floquet channels, it has only half the dimension of the original Floquet matrix (18). The entries in \mathcal{H}_e are themselves blocks of infinite dimension, in principle. They read explicitly

$$E_e = \begin{pmatrix} E_0 & 0 & 0 & \cdots \\ 0 & E_2 & 0 & \cdots \\ 0 & 0 & E_4 & \cdots \\ \vdots & \vdots & \vdots & \ddots \end{pmatrix}, \quad E_o = \begin{pmatrix} E_1 & 0 & 0 & \cdots \\ 0 & E_3 & 0 & \cdots \\ 0 & 0 & E_5 & \cdots \\ \vdots & \vdots & \vdots & \ddots \end{pmatrix}, \quad (24)$$

$$X_{eo} = \frac{S}{2} \begin{pmatrix} x_{0,1} & x_{0,3} & x_{0,5} & \cdots \\ x_{2,1} & x_{2,3} & x_{2,5} & \cdots \\ x_{4,1} & x_{4,3} & x_{4,5} & \cdots \\ \vdots & \vdots & \vdots & \ddots \end{pmatrix}, \quad X_{oe} = \frac{S}{2} \begin{pmatrix} x_{1,0} & x_{1,2} & x_{1,4} & \cdots \\ x_{3,0} & x_{3,2} & x_{3,4} & \cdots \\ x_{5,0} & x_{5,2} & x_{5,4} & \cdots \\ \vdots & \vdots & \vdots & \ddots \end{pmatrix}. \quad (25)$$

Here, E_e , E_o , represent the undriven Hamiltonian, and X_{eo} , X_{oe} the driving field $H_1 = Sx/2$, decomposed in the even and odd eigenstates $|\Psi_k\rangle$ of H_{DW} , with E_k denoting an eigenvalue of H_{DW} , and $x_{k,k'}$ a matrix element of the position operator, see Eq. (20).

2.2 Tunneling, driving, and dissipation

With the driving $H_F(t)$ switched off, the classical phase space generated by H_{DW} exhibits the constituent features of a bistable Hamiltonian system. A separatrix at $E = 0$ forms the border between two sets of trajectories: One set, with $E < 0$, comes in symmetry-related pairs, each partner of which oscillates in either one of the two potential minima. The other set consists of unpaired, spatially symmetric trajectories, with $E > 0$, which encircle both wells.

Torus quantization of the integrable undriven double well, Eq. (2), implies a simple qualitative picture of its eigenstates: The unpaired tori correspond to singlets with positive energy, whereas the symmetry-related pairs below the top of the barrier correspond to degenerate pairs of eigenstates. Due to the almost harmonic shape of the potential near its minima, neighboring pairs are separated in energy approximately by $\hbar\omega_0$. Exact quantization, however, predicts that the partners of these pairs have small but finite overlap. Therefore, the true eigenstates come in doublets, each of which consists of an even and an odd state, $|\Phi_n^+\rangle$ and $|\Phi_n^-\rangle$, respectively. The energies of the n th doublet are separated by a finite tunnel splitting Δ_n . We can always choose the global relative phase such that the superpositions

$$|\Phi_n^{\text{R,L}}\rangle = \frac{1}{\sqrt{2}} (|\Phi_n^+\rangle \pm |\Phi_n^-\rangle) \quad (26)$$

are localized in the right and the left well, respectively. As time evolves, the states $|\Phi_n^+\rangle$, $|\Phi_n^-\rangle$ acquire a relative phase $\exp(-i\Delta_n t/\hbar)$ and $|\Phi_n^{\text{R}}\rangle$, $|\Phi_n^{\text{L}}\rangle$ are transformed into one another after a time $\pi\hbar/\Delta_n$. Thus, the particle tunnels forth and back between the wells with a frequency Δ_n/\hbar . This introduces an additional, purely quantum-mechanical frequency scale, the tunnel rate Δ_0/\hbar of a particle residing in the ground-state doublet. Typically, tunnel rates are extremely small compared to the frequencies of the classical dynamics, all the more in the semiclassical regime we are interested in.

A driving of the form (3), even if its influence on the classical phase space is minor, can entail significant consequences for tunneling: It may enlarge the tunnel rate by orders of magnitude or even suppress tunneling altogether. For adiabatically slow driving, $\Omega \ll \Delta_0/\hbar$, tunneling is governed by the instantaneous tunnel splitting, which is always larger than its unperturbed value Δ_0 and results in an enhancement of the tunneling rate [33]. If the driving is faster, $\Delta_0/\hbar \lesssim \Omega \ll \omega_0$, cf. Fig. 2, the opposite holds true: The relevant time scale is now given by the inverse of the quasienergy splitting of the ground-state doublet $\hbar/|\epsilon_1 - \epsilon_0|$. It has been found [33,35] that in this case, for finite driving amplitude, $|\epsilon_1 - \epsilon_0| < \Delta_0$. Thus tunneling is always decelerated. Where the quasienergies of the ground-state doublet (which are of different generalized parity) intersect as a function of F , the splitting vanishes and tunneling is brought to a complete standstill by the purely coherent influence of the driving [32].

The small energy scales associated with tunneling make it extremely sensitive to any loss of coherence. As a consequence, the symmetry underlying the formation of tunnel doublets is generally broken, and an additional energy scale is introduced, the effective finite width attained by each discrete level. Tunneling and related coherence phenomena thus fade out on a time scale t_{decoh} . In general, this time scale gets shorter for higher temperatures, reflecting the growth of the transition rates (53) [36]. However, there exist counterintuitive effects: For driven tunneling in the vicinity of an exact crossing of the ground-state doublet, the coherent suppression of tunneling [22,32,33] can be stabilized with higher temperatures [37–39] until levels outside the doublet start to play a rôle.

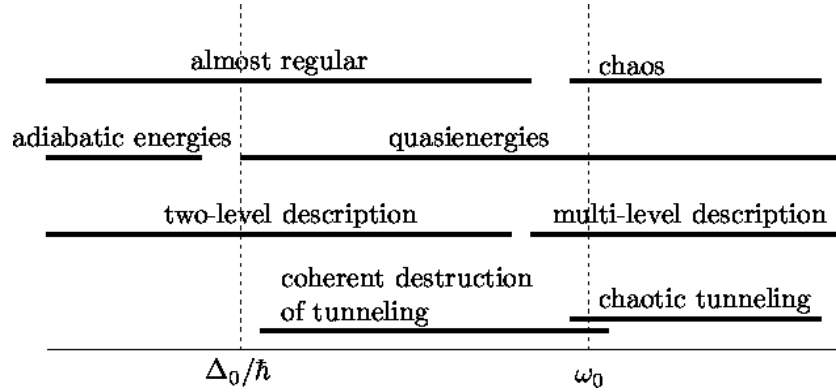


Fig. 2. Tunneling phenomena and the according appropriate levels of description for the non-dissipative driven double-well potential, Eq. (1). The bars depict the corresponding regimes of the driving frequency Ω . See Section 2 for a detailed discussion.

So far, we have considered only driving frequencies much smaller than the frequency scale ω_0 of the relevant classical resonances, i.e., a parameter regime where classical motion is predominantly regular. In this regime, coherent tunneling is well described within a two-state approximation [33,35]. In the dissipative case, however, a two-state approximation must fail for temperatures $k_B T \gtrsim \hbar\omega_0$, where thermal activation to higher doublets becomes relevant.

2.3 The onset of chaos

Driving with a frequency $\Omega \approx \omega_0$ affects also the dynamics of the classical bistable system, as small oscillations near the bottom of the wells become resonant with the driving and classical chaos comes into play (cf. Fig. 2). In a quantum description, this amounts to resonant multiple excitation of inter-doublet transitions until levels near the top of the barrier are significantly populated.

In this frequency regime, switching on the driving has two principal consequences for the classical dynamics: The separatrix is destroyed as a closed curve and replaced by a homoclinic tangle [40] of stable and unstable manifolds. A chaotic layer forms in the vicinity and with the topology of the former separatrix (cf. Fig. 6, below). This opens the way for diffusive transport between the two potential wells. Due to the nonlinearity of the potential, there is an infinite set of resonances of the driving with the unperturbed motion, both inside as well as outside the wells [41,42]. Since the period of the unperturbed, closed trajectories diverges for $E \rightarrow 0$, both from below and above, the resonances accumulate towards the separatrix of the unperturbed system. By its large phase-space area, the first resonance (the one for which the periods of the driving and of the unperturbed oscillation are in a 1-to-1 ratio) is prominent among the others and soon (in terms of increasing amplitude F) exceeds in size the “order-zero” regular areas near the bottom of each well [11].

Both major tendencies in the evolution of the classical phase space, extension of the chaotic layer and growth of the first resonance, leave their specific traces in the quasienergy spectrum. The tunnel doublets characterizing the unperturbed spectrum for $E < 0$ pertain to states located on pairs of symmetry-related quantizing tori in the regular regions within the wells. With increasing size of the chaotic layer, the quantizing tori one by one resolve in the chaotic sea. The corresponding doublets disappear as distinct structures in the spectrum as they attain a splitting of the same order as the mean level separation. The gradual widening of the doublets proceeds as a smooth function of the driving amplitude [11, 12], which roughly obeys a power law [43–45]. As soon as a pair of states is no longer supported by any torus-like manifold, including fractal [46] and vague tori [47], the corresponding eigenvalues detach themselves from the regular ladder to which they formerly belonged. They can then fluctuate freely in the spectrum and thereby “collide” with other chaotic singlets or regular doublets.

The appearance of a regular region, large enough to accommodate several eigenstates, around the first resonance introduces a second ladder of doublets into the spectrum. Size and shape of the first resonance vary in a way different from the main regular region. The corresponding doublet ladder therefore moves in the spectrum independently of the doublets that pertain to the main regular region, and of the chaotic singlets. This gives rise to additional singlet-doublet and even to doublet-doublet encounters.

3 Chaotic tunneling near singlet-doublet crossings

Near a crossing, level separations deviate vastly, in both directions, from the typical tunnel splitting (cf. Fig. 8, below). This is reflected in time-domain phenomena ranging from the suppression of tunneling to a strong increase in its rate and to complicated quantum beats [13–15]. Singlet-doublet crossings, in turn, drastically change the non-dissipative quasienergy scales and replace the two-level by a three-level structure. As a consequence, the familiar way tunneling fades out in the presence of dissipation is also significantly altered. Near a crossing, the coherent dynamics can last much longer than for the unperturbed doublet, despite the presence of the same dissipation as outside the crossing, establishing “chaos-induced coherence.” Depending on temperature, it can also be destroyed on a much shorter time scale.

For the parameters chosen in our numerical studies, higher resonances are negligible in size. Accordingly, the “coastal strip” between the chaotic layer along the former separatrix and the regular regions within and outside the wells, formed by hierarchies of regular islands around higher resonances, remains narrow (cf. Fig. 6). For the tunneling dynamics, the rôle of states located in the border region [17, 18] is therefore not significant in our case.

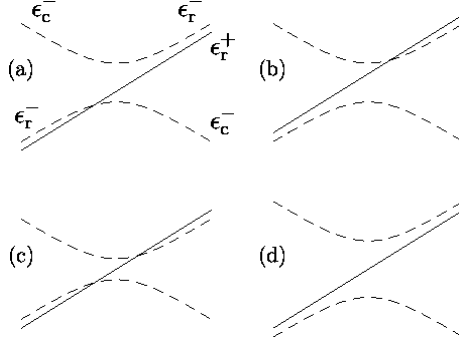


Fig. 3. Possible configurations of quasienergy crossings between a chaotic singlet and a regular doublet. Different line types signify different parity. See Section 3.1 for the labeling of the levels. Note that only for configurations (a),(b), the order of the regular doublet is restored in passing through the crossing. In configurations (c),(d), it is reversed.

3.1 Three-level crossings

Among the various types of quasienergy crossings that occur according to the above scenario, those involving a regular doublet and a chaotic singlet are the most common. In order to give a quantitative account of such crossings and the associated coherent dynamics, and for later reference in the context of the incoherent dynamics, we shall now discuss them in terms of a simple three-state model, devised much in the spirit of Ref. [7].

Far to the left of the crossing, we expect the following situation: There is a doublet of Floquet states

$$|\psi_r^+(t)\rangle = e^{-i\epsilon_r^+ t/\hbar} |\phi_r^+(t)\rangle, \quad (27)$$

$$|\psi_r^-(t)\rangle = e^{-i(\epsilon_r^+ + \Delta)t/\hbar} |\phi_r^-(t)\rangle, \quad (28)$$

with even (superscript +) and odd (−) generalized parity, respectively, residing on a pair of quantizing tori in one of the regular (subscript r) regions. We have assumed the quasienergy splitting $\Delta = \epsilon_r^- - \epsilon_r^+$ (as opposed to the unperturbed splitting) to be positive. The global relative phase is chosen such that the superpositions

$$|\phi_{R,L}(t)\rangle = \frac{1}{\sqrt{2}} (|\phi_r^+(t)\rangle \pm |\phi_r^-(t)\rangle) \quad (29)$$

are localized in the right and the left well, respectively, and tunnel back and forth with a frequency Δ/\hbar .

As the third player, we introduce a Floquet state

$$|\psi_c^-(t)\rangle = e^{-i(\epsilon_r^+ + \Delta + \Delta_c)t/\hbar} |\phi_c^-(t)\rangle, \quad (30)$$

located mainly in the chaotic (subscript c) layer, so that its time-periodic part $|\phi_c^-(t)\rangle$ contains a large number of harmonics. Without loss of generality, its parity is fixed to be odd. For the quasienergy, we assume that $\epsilon_c^- = \epsilon_r^+ + \Delta + \Delta_c = \epsilon_r^- + \Delta_c$, where $|\Delta_c|$ can be regarded as a measure of the distance from the crossing.

The structure of the classical phase space then implies that the mean energy of the chaotic state should be close to the top of the barrier and far above that of the doublet. We assume, like for the quasienergies, a small splitting of the mean energies pertaining to the regular doublet, $|E_r^- - E_r^+| \ll E_c^- - E_r^\pm$.

In order to model an avoided crossing between $|\phi_r^-\rangle$ and $|\phi_c^-\rangle$, we suppose that there is a non-vanishing fixed matrix element

$$b = \langle\langle \phi_r^- | H_{\text{DW}} | \phi_c^- \rangle\rangle > 0. \quad (31)$$

For the singlet-doublet crossings under study, we typically find that $\Delta \ll b \ll \hbar\Omega$. Neglecting the coupling with all other states, we model the system by the three-state (subscript 3s) Floquet Hamiltonian

$$\mathcal{H}_{3s} = \epsilon_r^+ + \begin{pmatrix} 0 & 0 & 0 \\ 0 & \Delta & b \\ 0 & b & \Delta + \Delta_c \end{pmatrix} \quad (32)$$

in the three-dimensional Hilbert space spanned by $\{|\phi_r^+(t)\rangle, |\phi_r^-(t)\rangle, |\phi_c^-(t)\rangle\}$. Its Floquet states are

$$\begin{aligned} |\phi_0^+(t)\rangle &= |\phi_r^+(t)\rangle, \\ |\phi_1^-(t)\rangle &= (|\phi_r^-(t)\rangle \cos \beta - |\phi_c^-(t)\rangle \sin \beta), \\ |\phi_2^-(t)\rangle &= (|\phi_r^-(t)\rangle \sin \beta + |\phi_c^-(t)\rangle \cos \beta). \end{aligned} \quad (33)$$

with quasienergies

$$\epsilon_0^+ = \epsilon_r^+, \quad \epsilon_{1,2}^- = \epsilon_r^+ + \Delta + \frac{1}{2}\Delta_c \mp \frac{1}{2}\sqrt{\Delta_c^2 + 4b^2}, \quad (34)$$

and mean energies, neglecting contributions of the matrix element b ,

$$\begin{aligned} E_0^+ &= E_r^+, \\ E_1^- &= E_r^- \cos^2 \beta + E_c^- \sin^2 \beta, \\ E_2^- &= E_r^- \sin^2 \beta + E_c^- \cos^2 \beta. \end{aligned} \quad (35)$$

The angle β describes the mixing between the Floquet states $|\phi_r^-\rangle$ and $|\phi_c^-\rangle$ and is an alternative measure of the distance to the avoided crossing. By diagonalizing the Hamiltonian (32), we obtain

$$2\beta = \arctan\left(\frac{2b}{\Delta_c}\right), \quad 0 < \beta < \frac{\pi}{2}. \quad (36)$$

For $\beta \rightarrow \pi/2$, corresponding to $-\Delta_c \gg b$, we retain the situation far left of the crossing, as outlined above, with $|\phi_1^-\rangle \approx |\phi_c^-\rangle$, $|\phi_2^-\rangle \approx |\phi_r^-\rangle$. To the far right of the crossing, i.e., for $\beta \rightarrow 0$ or $\Delta_c \gg b$, the exact eigenstates $|\phi_1^-\rangle$ and $|\phi_2^-\rangle$ have interchanged their phase-space structure [13–15]. Here, we have $|\phi_1^-\rangle \approx |\phi_r^-\rangle$ and $|\phi_2^-\rangle \approx |\phi_c^-\rangle$. The mean energy is essentially determined by this phase-space structure, so that there is also an exchange of E_1^- and E_2^- in an exact crossing,

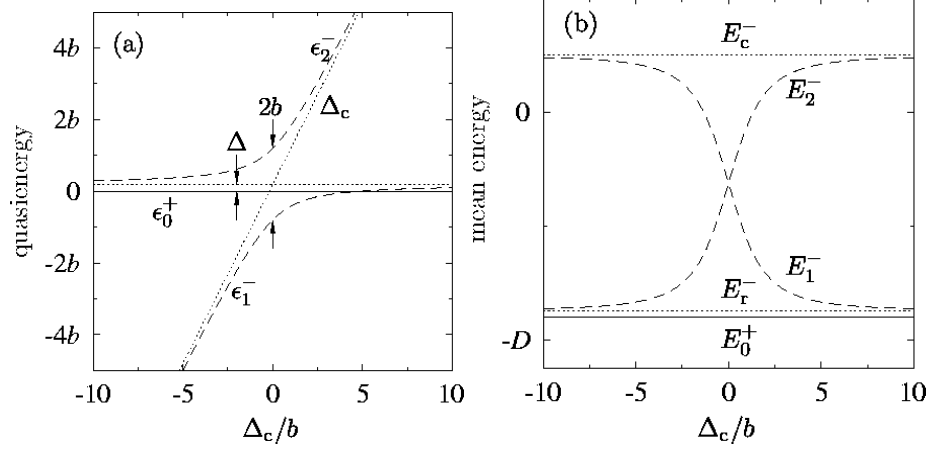


Fig. 4. A singlet-doublet crossing, according to the three-state model (32), in terms of the quasienergies (a) and the mean energies (b) as functions of the coupling parameter Δ_c/b . Energies for a corresponding exact crossing (i.e., with the crossing states uncoupled) are marked by dotted lines, the energies in the presence of coupling by full and dashed lines for even and odd states, respectively.

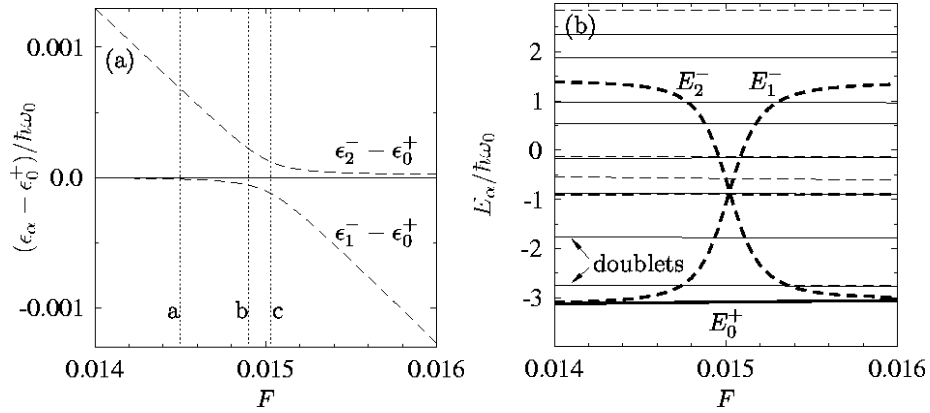


Fig. 5. Singlet-doublet crossing found numerically for the driven double well, Eq. (1), at $D = 4$ and $\Omega = 0.982\omega_0$, in terms of the dependence of the quasienergies (a) and the mean energies (b) on the driving amplitude F . Values of the driving amplitude used in Fig. 9 are marked by the dotted vertical lines. Full and dashed lines indicate energies of even and odd states, respectively. Bold lines give the mean energies of the chaotic singlet and the ground-state doublet depicted in panel (a).

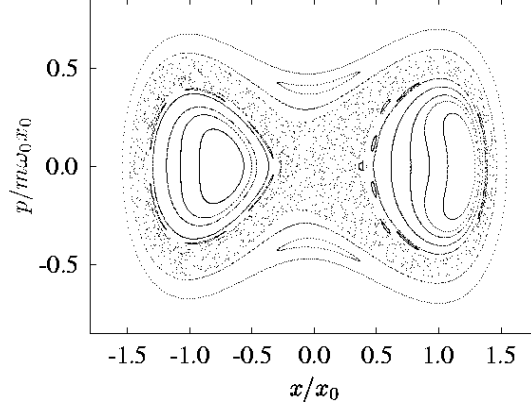


Fig. 6. Classical stroboscopic phase space portrait, at $t = 2\pi n/\Omega$, of the harmonically driven quartic double well, Eq. (1). The driving parameters $F = 0.015$, $\Omega = 0.982\omega_0$, are at the center of the singlet-doublet crossing shown in Fig. 5.

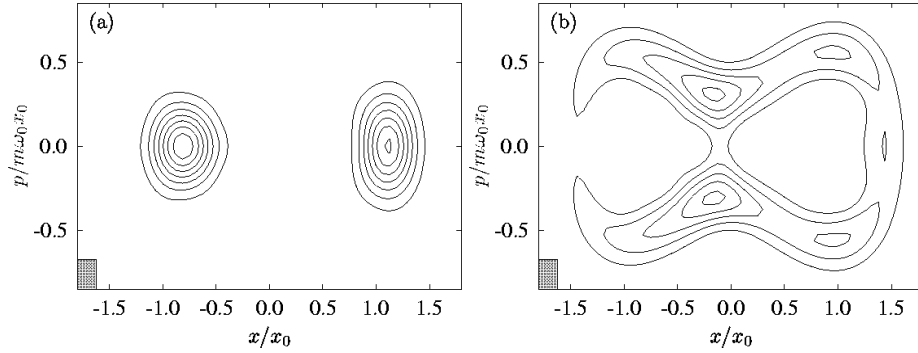


Fig. 7. Contour plots of the Husimi functions for the Floquet states $|\phi_1^-\rangle \approx |\phi_r^-\rangle$ (a) and $|\phi_2^-\rangle \approx |\phi_c^-\rangle$ (b) of the harmonically driven quartic double well, Eq. (1), at stroboscopic times $t = nP$. The driving parameters $F = 0.014$, $\Omega = 0.982\omega_0$, are in sufficient distance to the singlet-doublet crossing such that the admixture from the chaotic singlet state is negligible. The rectangle in the lower left corner has the size of the effective quantum of action \hbar_{eff} .

cf. Eq. (35), while E_0^+ remains unaffected (Fig. 4b). The quasienergies ϵ_0^+ and ϵ_1^- must intersect close to the avoided crossing of ϵ_1^- and ϵ_2^- (Fig. 4a). Their crossing is exact, since they pertain to states with opposite parity (cf. Fig. 3a,b).

In order to illustrate the above three-state model and to demonstrate its adequacy, we have numerically studied a singlet-doublet crossing that occurs for the double-well potential, Eq. (1), with $D = 4$, at a driving frequency $\Omega = 0.982\omega_0$ and amplitude $F = 0.015029$ (Fig. 5). The phase-space structure of the participating Floquet states (Figs. 6, 7) meets the assumptions of our three-state

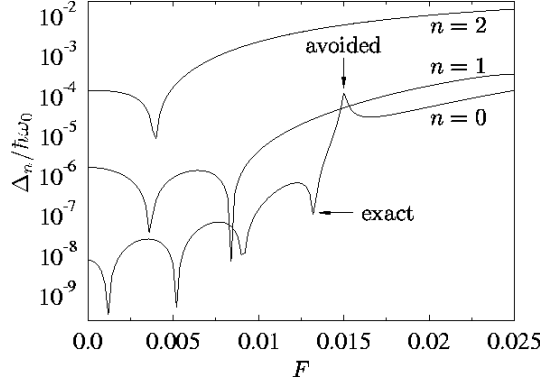


Fig. 8. Splitting of the lowest doublets for $D = 4$ and $\Omega = 0.982\omega_0$. The arrows indicate the locations of the exact and the avoided crossing within a three-level crossing of the type sketched in Fig. 3a.

theory. A comparison of the appropriately scaled three-state theory (Fig. 4) with this real singlet-doublet crossing (Fig. 5) shows satisfactory agreement. Note that in the real crossing, the quasienergy of the chaotic singlet *decreases* as a function of F , so that the exact crossing occurs to the left of the avoided one. This numerical example also shows a deficiency of the idealized three-state model. Following the global tendency of widening of the splittings with increasing driving amplitude [11, 44, 45], it may happen that even far away from a crossing, the doublet splitting does not return to its value on the opposite side (see Fig. 8). It is even possible that an exact crossing of ϵ_0^+ and ϵ_1^- never takes place in the vicinity of the crossing. In that case, the relation of the quasienergies in the doublet gets reversed via the crossing (Fig. 3c,d). Nevertheless, the three-state scenario captures the essential features.

To study the dynamics of the tunneling process, we focus on the state

$$|\psi(t)\rangle = \frac{1}{\sqrt{2}} \left(e^{-i\epsilon_0^+ t/\hbar} |\phi_0^+(t)\rangle + e^{-i\epsilon_1^- t/\hbar} |\phi_1^-(t)\rangle \cos \beta + e^{-i\epsilon_2^- t/\hbar} |\phi_2^-(t)\rangle \sin \beta \right). \quad (37)$$

It is constructed such that at $t = 0$, it corresponds to the decomposition of $|\phi_R\rangle$ in the basis (33) at finite distance from the crossing. Therefore, it is initially localized in the regular region in the right well and follows the time evolution under the Hamiltonian (32). From Eqs. (29), (33), we find the probabilities for its evolving into $|\phi_R\rangle$, $|\phi_L\rangle$, or $|\phi_c\rangle$, respectively, to be

$$\begin{aligned} P_{R,L}(t) &= |\langle \phi_{R,L}(t) | \psi(t) \rangle|^2 \\ &= \frac{1}{2} \left(1 \pm \left[\cos \frac{(\epsilon_1^- - \epsilon_0^+)t}{\hbar} \cos^2 \beta + \cos \frac{(\epsilon_2^- - \epsilon_0^+)t}{\hbar} \sin^2 \beta \right] \right. \\ &\quad \left. + \left[\cos \frac{(\epsilon_1^- - \epsilon_2^-)t}{\hbar} - 1 \right] \cos^2 \beta \sin^2 \beta \right), \quad (38) \\ P_c(t) &= |\langle \phi_c(t) | \psi(t) \rangle|^2 = \left[1 - \cos \frac{(\epsilon_1^- - \epsilon_2^-)t}{\hbar} \right] \cos^2 \beta \sin^2 \beta. \end{aligned}$$

We discuss the coherent dynamics of the three-state model for different distances to the crossing and illustrate it by numerical results for the real crossing introduced above.

At sufficient distance from the crossing, there is only little mixing between the regular and the chaotic states, i.e., $\sin \beta \ll 1$ or $\cos \beta \ll 1$. The tunneling process then follows the familiar two-state dynamics involving only $|\phi_r^+\rangle$ and $|\phi_r^-\rangle$, with tunnel frequency Δ/\hbar (Fig. 9a). Close to the avoided crossing, $\cos \beta$ and $\sin \beta$ are of the same order of magnitude, and $|\phi_1^-\rangle$, $|\phi_2^-\rangle$ become very similar to one another. Both now have support in the chaotic layer as well as in the symmetry-related regular regions, they are of a hybrid nature. Here, the tunneling involves all the three states and must be described at least by a three-level system. The exchange of probability between the two regular regions proceeds via a “stop-over” in the chaotic region [7, 8, 13–15].

The three quasienergy differences that determine the time scales of this process are in general all different, leading to complicated beats (Fig. 9b). However, for $\Delta_c = -2\Delta$, the two quasienergies $\epsilon_1^- - \epsilon_0^+$ and $\epsilon_0^+ - \epsilon_2^-$ are degenerate. At this point, the center of the crossing, the number of different frequencies in the three-level dynamics reduces to two again. This restores the familiar coherent tunneling in the sense that there is again a simple periodic exchange of probability between the regular regions [13–15]. However, the rate is much larger if compared to the situation far off the crossing, and the chaotic region is now temporarily populated during each probability transfer, twice per tunneling cycle (Fig. 9c).

4 Incoherent quantum dynamics

4.1 Master equation

System-bath model. To achieve a microscopic model of dissipation, we couple the system (1) bilinearly to a bath of non-interacting harmonic oscillators [48, 49]. The total Hamiltonian of system and bath is then given by

$$H(t) = H_{\text{DW}}(t) + \sum_{\nu=1}^{\infty} \left(\frac{p_{\nu}^2}{2m_{\nu}} + \frac{m_{\nu}}{2} \omega_{\nu}^2 \left(x_{\nu} - \frac{g_{\nu}}{m_{\nu} \omega_{\nu}^2} x \right)^2 \right). \quad (39)$$

The position x of the system is coupled, with coupling strength g_{ν} , to an ensemble of oscillators with masses m_{ν} , frequencies ω_{ν} , momenta p_{ν} , and coordinates x_{ν} . The bath is fully characterized by the spectral density of the coupling energy,

$$J(\omega) = \pi \sum_{\nu=1}^{\infty} \frac{g_{\nu}^2}{2m_{\nu} \omega_{\nu}} \delta(\omega - \omega_{\nu}). \quad (40)$$

For the time evolution we choose an initial condition of the Feynman-Vernon type: at $t = t_0$, the bath is in thermal equilibrium and uncorrelated to the system, i.e.,

$$\rho(t_0) = \rho_S(t_0) \otimes \rho_{\text{B,eq}}, \quad (41)$$

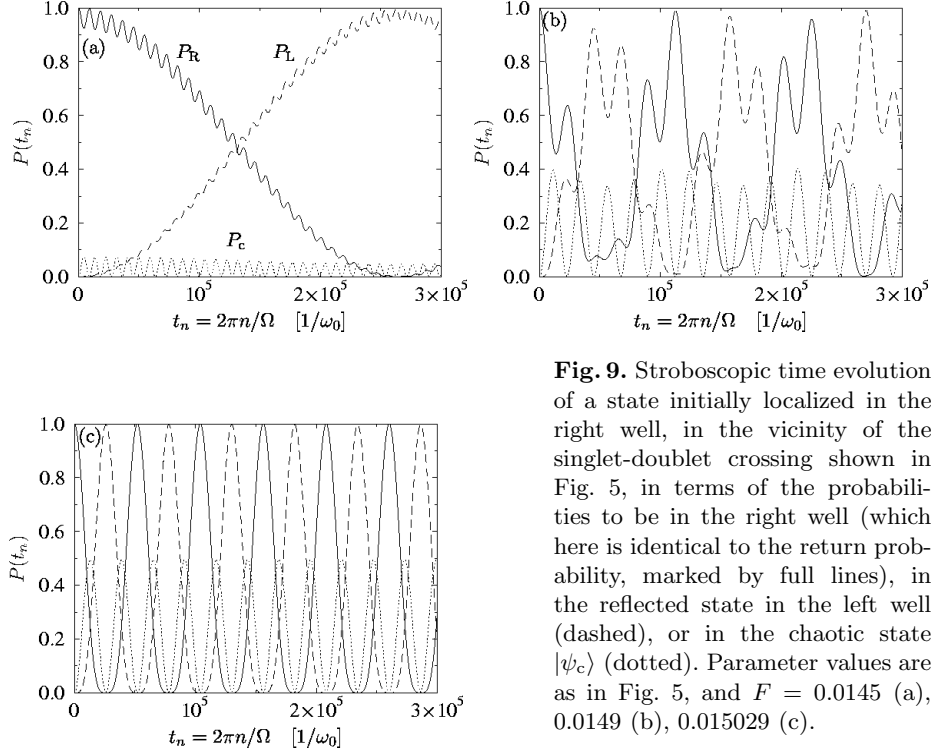


Fig. 9. Stroboscopic time evolution of a state initially localized in the right well, in the vicinity of the singlet-doublet crossing shown in Fig. 5, in terms of the probabilities to be in the right well (which here is identical to the return probability, marked by full lines), in the reflected state in the left well (dashed), or in the chaotic state $|\psi_c\rangle$ (dotted). Parameter values are as in Fig. 5, and $F = 0.0145$ (a), 0.0149 (b), 0.015029 (c).

where $\rho_{B,\text{eq}} = \exp(-\beta H_B)/\text{tr}_B \exp(-\beta H_B)$ is the canonical ensemble of the bath and $1/\beta = k_B T$.

Due to the bilinearity of the system–bath coupling, one can always eliminate the bath variables to get an exact, closed integro-differential equation for the reduced density matrix $\rho_S(t) = \text{tr}_B \rho(t)$. It describes the dynamics of the central system, subject to dissipation [50].

Born-Markov approximation. In most cases, however, the integro-differential equation for $\rho_S(t)$ can be solved only approximately. In particular, in the limit of weak coupling,

$$\gamma \ll k_B T/\hbar, \quad (42)$$

$$\gamma \ll |\epsilon_\alpha - \epsilon_{\alpha'}|/\hbar, \quad (43)$$

it is possible to truncate the time-dependent perturbation expansion in the system–bath interaction after the second-order term. The quantity γ , to be defined below, denotes the effective damping of the dissipative system, and $|\epsilon_\alpha - \epsilon_{\alpha'}|/\hbar$ are the transition frequencies of the central system. In the present case, *the central system is understood to include the driving* [51–54], so that

the transition frequencies are given by quasienergy differences. The autocorrelations of the bath decay on a time scale $\hbar/k_B T$ and thus in the present limit, instantaneously on the time scale $1/\gamma$ of the system correlations. With the initial preparation (41), the equation of motion for the reduced density matrix in this approximation is given by [54]

$$\begin{aligned} \dot{\rho}_S(t) = & -\frac{i}{\hbar} [H_S(t), \rho_S(t)] + \frac{1}{\pi\hbar} \int_{-\infty}^{\infty} d\omega J(\omega) n_{\text{th}}(\hbar\omega) \\ & \times \int_0^{\infty} d\tau (e^{i\omega\tau} [\tilde{x}(t-\tau, t)\rho_S(t), x] + \text{H.c.}), \end{aligned} \quad (44)$$

where $\tilde{x}(t', t)$ denotes the position operator in the interaction picture defined by

$$\tilde{x}(t', t) = U^\dagger(t', t) x U(t', t), \quad (45)$$

with $U(t', t)$, the propagator of the conservative driven double well, given in Eq. (12). ‘H.c.’ means ‘Hermitian conjugate’, and

$$n_{\text{th}}(\epsilon) = \frac{1}{e^{\epsilon/k_B T} - 1} = -n_{\text{th}}(-\epsilon) - 1 \quad (46)$$

is the thermal occupation of the bath oscillator with energy ϵ . To achieve a more compact notation, we require $J(-\omega) = -J(\omega)$. In the following, we shall restrict ourselves to an Ohmic bath, $J(\omega) = m\gamma\omega$. This defines the effective damping constant γ .

We use the time-periodic components $|\phi_\alpha(t)\rangle$ of the Floquet states as a basis to expand the density operator, Eq. (44). Expressing the matrix elements

$$X_{\alpha\beta}(t) = \langle \phi_\alpha(t) | x | \phi_\beta(t) \rangle \quad (47)$$

of the position operator by their Fourier coefficients

$$X_{\alpha\beta, n} = \langle \langle \phi_\alpha(t) | x e^{-in\Omega t} | \phi_\beta(t) \rangle \rangle = X_{\beta\alpha, -n}^*, \quad (48)$$

$$X_{\alpha\beta}(t) = \sum_n e^{in\Omega t} X_{\alpha\beta, n}, \quad (49)$$

yields the equation of motion for the elements $\rho_{\alpha\beta}$ of the reduced density matrix ρ_S [37, 39, 52, 54],

$$\begin{aligned} \dot{\rho}_{\alpha\beta}(t) = & \frac{d}{dt} \langle \phi_\alpha(t) | \rho_S(t) | \phi_\beta(t) \rangle \\ = & -\frac{i}{\hbar} (\epsilon_\alpha - \epsilon_\beta) \rho_{\alpha\beta}(t) \\ & + \sum_{\alpha'\beta'nn'} (N_{\alpha\alpha', n} X_{\alpha\alpha', n} \rho_{\alpha'\beta'} X_{\beta'\beta, n'} \\ & - N_{\alpha'\beta', n} X_{\alpha\alpha', n'} X_{\alpha\alpha', n} \rho_{\beta'\beta}) e^{i(n+n')\omega t} + \text{H.c.} \end{aligned} \quad (50)$$

The coefficients of this differential equation are periodic in time with the period of the driving. The $N_{\alpha\beta,n}$ are given by

$$N_{\alpha\beta,n} = N(\epsilon_\alpha - \epsilon_\beta + n\hbar\Omega), \quad N(\epsilon) = \frac{m\gamma\epsilon}{\hbar^2} n_{\text{th}}(\epsilon). \quad (51)$$

For $\epsilon \gg k_B T$, $N(\epsilon)$ approaches zero.

Since the position operator x is odd under P_P (cf. Eq. (22)), the master equations (44) and (50) are invariant under P_P . Therefore, both the conservative and the dissipative dynamics preserve the parity of the operator $|\phi_\alpha\rangle\langle\phi_\beta|$. If $|\phi_\alpha\rangle$ and $|\phi_\beta\rangle$ belong to the same parity class, it is even, and odd otherwise. In particular, the projectors $|\phi_\alpha\rangle\langle\phi_\alpha|$ and thus all density matrices diagonal in the Floquet basis are even under P_P .

Rotating-wave approximation. Assuming that dissipative effects are relevant only on a time scale much larger than the period P of the driving, we average the coefficients of the master equation (50) over P to obtain the equation of motion

$$\dot{\rho}_{\alpha\beta}(t) = -\frac{i}{\hbar}(\epsilon_\alpha - \epsilon_\beta)\rho_{\alpha\beta}(t) + \sum_{\alpha'\beta'} \mathcal{L}_{\alpha\beta,\alpha'\beta'} \rho_{\alpha'\beta'}, \quad (52)$$

with the time-independent dissipative part

$$\begin{aligned} \mathcal{L}_{\alpha\beta,\alpha'\beta'} &= \sum_n (N_{\alpha\alpha',n} + N_{\beta\beta',n}) X_{\alpha\alpha',n} X_{\beta'\beta,-n} \\ &\quad - \delta_{\beta\beta'} \sum_{\beta'',n} N_{\beta''\alpha',n} X_{\alpha\beta'',-n} X_{\beta''\alpha',n} \\ &\quad - \delta_{\alpha\alpha'} \sum_{\alpha'',n} N_{\alpha''\beta',n} X_{\beta'\alpha'',-n} X_{\alpha''\beta,n}. \end{aligned} \quad (53)$$

This step amounts to a rotating-wave approximation which is, however, less restrictive than the one introduced in [51,52] where dissipative effects are averaged over the generally longer time scale $\max_{\alpha,\beta,n}(2\pi\hbar/(\epsilon_\alpha - \epsilon_\beta + n\hbar\Omega))$.

4.2 Chaos-assisted dissipative tunneling

The crucial effect of dissipation on a quantum system is the disruption of coherence: a coherent superposition evolves into an incoherent mixture. Thus, phenomena based on coherence, such as tunneling, are rendered transients that fade out on a finite time scale t_{decoh} . In general, for driven tunneling in the weakly damped regime, this time scale gets shorter for higher temperatures, as transition rates grow [36]. However, in the vicinity of an exact crossing of the ground-state quasienergies, the coherent suppression of tunneling [22,32,33] can be stabilized with higher temperatures [37–39] and increasing friction [55,56] until levels outside the doublet start to play a rôle. We have studied dissipative chaos-assisted

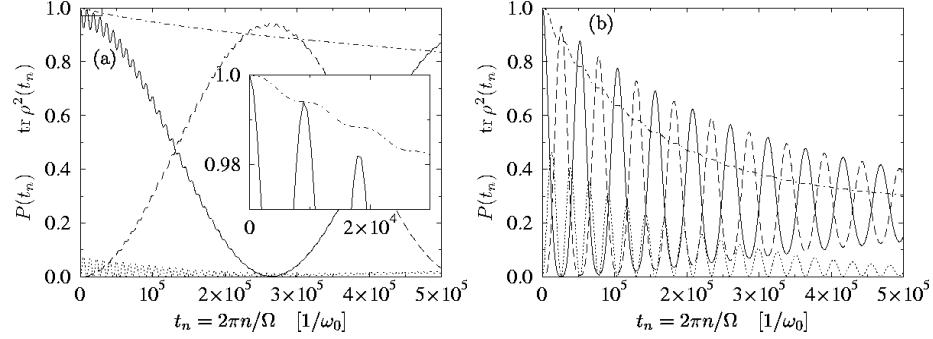


Fig. 10. Occupation probabilities as in Fig. 9a,c, but in the presence of dissipation. The dash-dotted line shows the time evolution of $\text{tr } \rho^2$. The parameter values are $D = 4$, $\Omega = 0.982 \omega_0$, $\gamma = 10^{-6} \omega_0$, $k_B T = 10^{-4} \hbar \omega_0$, and $F = 0.0145$ (a), 0.015029 (b). The inset in (a) is a blow up of the rectangle in the upper left corner of that panel.

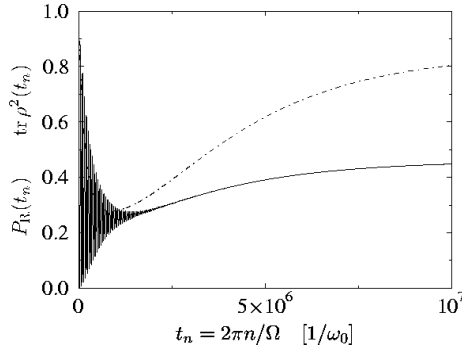


Fig. 11. Time evolution of the return probability P_R (full line) and the coherence function $\text{tr } \rho^2$ (dash-dotted) during loss and regain of coherence. The parameter values are as in Fig. 10b.

tunneling, at the particular real singlet-doublet crossing introduced in Sec. 3.1 (see Fig. 5). The time evolution has been computed numerically by iterating the dissipative quantum map for the improved master equation in moderate rotating-wave approximation, Eq. (52). As initial condition, we have chosen the density operator $\rho(0) = |\phi_R\rangle\langle\phi_R|$, a pure state located in the right well.

In the vicinity of a singlet-doublet crossing, the tunnel splitting increases significantly—the essence of chaos-assisted tunneling. During the tunneling, the chaotic singlet $|\phi_c\rangle$ becomes populated periodically with frequency $|\epsilon_2^- - \epsilon_1^-|/\hbar$, cf. Eq. (38) and Fig. 9. The high mean energy of this singlet results in an enhanced decay of coherence at times when it is well populated (Fig. 10). For the relaxation towards the asymptotic state, also the slower transitions within doublets are relevant. Therefore, the corresponding time scale t_{relax} can be much larger than t_{decoh} (Fig. 11).

To obtain quantitative estimates for the dissipative time scales, we approximate t_{decoh} by the decay rate of $\text{tr } \rho^2$, as a measure of coherence, averaged over

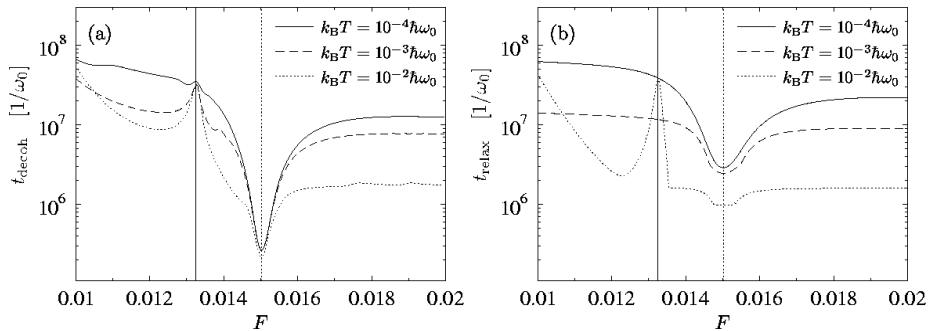


Fig. 12. Time scales of the decay of the coherence measure $\text{tr} \rho^2$ (a) and of the relaxation towards the asymptotic solution (b) near the singlet-doublet crossing. Near the exact crossing ($F \approx 0.013$, full vertical line) coherence is stabilized, whereas at the center of the avoided crossing ($F \approx 0.015$, dashed vertical line) the decay of coherence is accelerated. The parameter values are $D = 4$, $\Omega = 0.982 \omega_0$, $\gamma = 10^{-6} \omega_0$, temperature as given in the legend.

a time t_p ,

$$\frac{1}{t_{\text{decoh}}} = -\frac{1}{t_p} \int_0^{t_p} dt' \frac{d}{dt'} \text{tr} \rho^2(t') \quad (54)$$

$$= \frac{1}{t_p} \left(\text{tr} \rho^2(0) - \text{tr} \rho^2(t_p) \right). \quad (55)$$

Because of the stepwise loss of coherence (Fig. 10), we have chosen the propagation time t_p as an n fold multiple of the duration $2\pi\hbar/|\epsilon_2^- - \epsilon_1^-|$ of the chaotic beats. For this procedure to be meaningful, n should be so large that the coherence decays substantially during the time t_p (in our numerical studies to a value of approximately 0.9). The time scale t_{relax} of the approach to the asymptotic state is given by the reciprocal of the smallest real part of the eigenvalues of the dissipative kernel.

Outside the singlet-doublet crossing we find that the decay of coherence and the relaxation take place on roughly the same time scale (Fig. 12). At $F \approx 0.013$, the chaotic singlet induces an exact crossing of the ground-state quasienergies (see Fig. 8), resulting in a *stabilization of coherence* with increasing temperature. At the center of the avoided crossing, the decay of coherence becomes much faster and is essentially independent of temperature. This indicates that transitions from states with mean energy far above the ground state play a crucial rôle.

4.3 Asymptotic state

As the dynamics described by the master equation (52) is dissipative, it converges in the long-time limit to an asymptotic state $\rho_\infty(t)$. In general, this attractor remains time dependent but shares the symmetries of the central system, i.e.

here, periodicity and generalized parity. However, the coefficients (53) of the master equation for the matrix elements $\rho_{\alpha\beta}$, valid within a moderate rotating-wave approximation, are time independent and so the asymptotic solution also is. The explicit time dependence of the attractor has been effectively eliminated by representing it in the Floquet basis and introducing a mild rotating-wave approximation.

To gain some qualitative insight into the asymptotic solution, we focus on the diagonal elements

$$\mathcal{L}_{\alpha\alpha,\alpha'\alpha'} = 2 \sum_n N_{\alpha\alpha',n} |X_{\alpha\alpha',n}|^2, \quad \alpha \neq \alpha', \quad (56)$$

of the dissipative kernel. They give the rates of direct transitions from $|\phi_{\alpha'}\rangle$ to $|\phi_{\alpha}\rangle$. Within a full rotating-wave approximation [51,52], these were the only non-vanishing contributions to the master equation to affect the diagonal elements $\rho_{\alpha\alpha}$ of the density matrix.

In the case of zero driving amplitude, the Floquet states $|\phi_{\alpha}\rangle$ reduce to the eigenstates of the undriven Hamiltonian H_{DW} . The only non-vanishing Fourier component is then $|c_{\alpha,0}\rangle$, and the quasienergies ϵ_{α} reduce to the corresponding eigenenergies E_{α} . Thus $\mathcal{L}_{\alpha\alpha,\alpha'\alpha'}$ only consists of a single term proportional to $N(\epsilon_{\alpha} - \epsilon_{\alpha'})$. It describes two kinds of thermal transitions: decay to states with lower energy and, if the energy difference is less than $k_{\text{B}}T$, thermal activation to states with higher energy. The ratio of the direct transitions forth and back then reads

$$\frac{\mathcal{L}_{\alpha\alpha,\alpha'\alpha'}}{\mathcal{L}_{\alpha'\alpha',\alpha\alpha}} = \exp\left(-\frac{\epsilon_{\alpha} - \epsilon_{\alpha'}}{k_{\text{B}}T}\right). \quad (57)$$

We have detailed balance and therefore the steady-state solution is

$$\rho_{\alpha\alpha'}(\infty) \sim e^{-\epsilon_{\alpha}/k_{\text{B}}T} \delta_{\alpha\alpha'}. \quad (58)$$

In particular, the occupation probability decays monotonically with the energy of the eigenstates. In the limit $k_{\text{B}}T \rightarrow 0$, the system tends to occupy the ground state only.

For a strong driving, each Floquet state $|\phi_{\alpha}\rangle$ contains a large number of Fourier components and $\mathcal{L}_{\alpha\alpha,\alpha'\alpha'}$ is given by a sum over contributions with quasienergies $\epsilon_{\alpha} - \epsilon_{\alpha'} + n\hbar\Omega$. Thus decay to states with ‘‘higher’’ quasienergy (recall that quasienergies do not allow for a global ordering) becomes possible due to terms with $n < 0$. Physically, it amounts to an incoherent transition under absorption of driving-field quanta. Correspondingly, the system tends to occupy Floquet states comprising many Fourier components with low index n . According to Eq. (16), these states have a low mean energy.

The effects under study are found for a driving with a frequency of the order of unity. Thus for a quasienergy doublet, not close to a crossing, we have $|\epsilon_{\alpha} - \epsilon_{\alpha'}| \ll \hbar\Omega$, and $\mathcal{L}_{\alpha'\alpha',\alpha\alpha}$ is dominated by contributions with $n < 0$, where the splitting has no significant influence. However, up to the tunnel splitting, the two partners in the quasienergy doublet are almost identical. Therefore, with

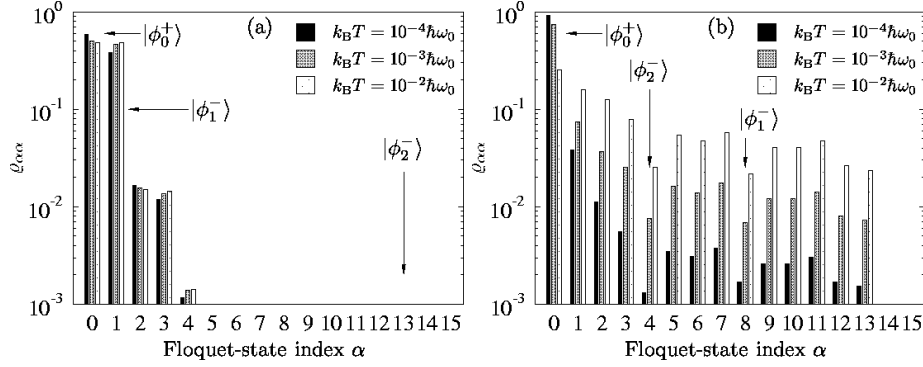


Fig. 13. Occupation probability $\rho_{\alpha\alpha}$ of the Floquet states $|\phi_\alpha\rangle$ in the long-time limit. The parameter values are $D = 4$, $\Omega = 0.982\omega_0$, $\gamma = 10^{-6}\omega_0$, and $F = 0.013$ (a), 0.015029 (b), temperature as given in the legend.

respect to dissipation, both should behave similarly. In particular, one expects an equal population of the doublets even in the limit of zero temperature (Fig. 13a), in contrast to the time-independent case.

In the vicinity of a singlet-doublet crossing the situation is more subtle. Here, the odd partner, say, of the doublet mixes with a chaotic singlet, cf. Eq. (33), and thus acquires components with higher energy. Due to the high mean energy E_c^- of the chaotic singlet, close to the top of the barrier, the decay back to the ground state can also proceed indirectly via other states with mean energy below E_c^- . Thus $|\phi_1^- \rangle$ and $|\phi_2^- \rangle$ are depleted and mainly $|\phi_0^+ \rangle$ will be populated. However, if the temperature is significantly above the splitting $2b$ at the avoided crossing, thermal activation from $|\phi_0^+ \rangle$ to $|\phi_{1,2}^- \rangle$, accompanied by depletion via the states below E_c^- , becomes possible. Thus asymptotically, all these states become populated in a steady closed flow (Fig. 13b). The long-time limit of the corresponding classical dynamics converges to one of two limit cycles, each of which is located close to one of the potential minima. In a stroboscopic map they correspond to two isolated fixed points. This behavior is qualitatively different from the asymptotic limit of the dissipative quantum dynamics near the center of the crossing and shows that the occupation of levels outside the singlet and the doublet for $t \rightarrow \infty$ is a pure quantum effect.

Important global characteristics of the asymptotic state, measuring its degree of spreading over phase space, are the Shannon entropy $S = -\text{tr}(\rho_\infty \ln \rho_\infty)$ or, alternatively, $\text{tr} \rho_\infty^2$. The latter gives approximately the inverse number of incoherently occupied states and can be considered an “incoherent inverse participation ratio” [57]. It equals unity only if the attractor is a pure state. According to the above scenario, we expect $\text{tr} \rho_\infty^2$ to assume the value $1/2$, in a regime with strong driving but preserved doublet structure, reflecting the incoherent population of the ground-state doublet. In the vicinity of the singlet-doublet crossing where the doublet structure is dissolved, its value should be close to unity for

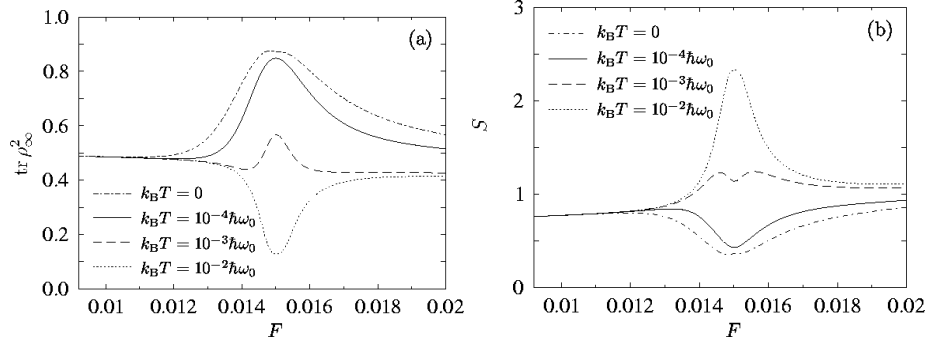


Fig. 14. Coherence (a) and Shannon entropy (b) of the asymptotic state in the vicinity of a singlet-doublet crossing for different temperatures as given in the legend. The other parameter values are $D = 4$, $\Omega = 0.982 \omega_0$, and $\gamma = 10^{-6} \omega_0$.

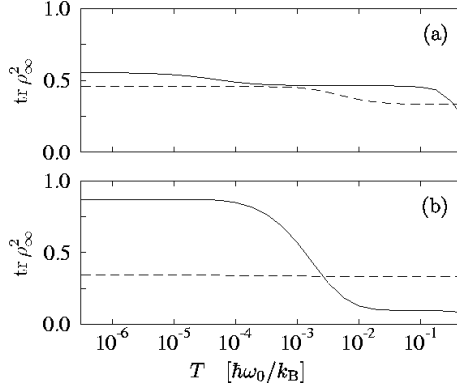


Fig. 15. Coherence of the asymptotic state in the vicinity of a singlet-doublet crossing for $F = 0.013$ (a) and $F = 0.015029$ (b): exact calculation (full line) compared to the result of a three-level description (dashed) of the dissipative dynamics. The other parameter values are $D = 4$, $\Omega = 0.982 \omega_0$, and $\gamma = 10^{-6} \omega_0$.

temperatures $k_B T \ll 2b$ and much less than unity for $k_B T \gg 2b$ (Figs. 14a, 15). This means that the crossing of the chaotic singlet with the regular doublet leads to an improvement of coherence if the temperature is below the splitting of the avoided crossing, and to a loss for temperatures above the splitting. This phenomenon amounts to a *chaos-induced* coherence or incoherence, respectively. The corresponding Shannon entropy (Fig. 14b) assumes approximately the value $\ln n$ for n incoherently populated states. Thus outside the crossing, we have $S \approx \ln 2$ and at the center of the crossing the entropy exhibits a significant temperature dependence.

The crucial rôle of the decay via states not involved in the three-level crossing can be demonstrated by comparing it to the dissipative dynamics including only these three levels (plus the bath). At the crossing, the three-state model results in a completely different type of asymptotic state (Fig. 15). The failure of the three-state model in the presence of dissipation clearly indicates that in the vicinity of the singlet-doublet crossing, it is important to take a large set of levels into account.

5 Signatures of chaos in the asymptotic state

Phase-space representations of quantum mechanics, like the Husimi or the Wigner distributions, help to reveal the structures of the corresponding classical phase space [7, 58–62]. In particular, for the case of regular classical dynamics, the Husimi function of a (quasi)energy eigenstate is localized along the corresponding quantizing torus; for chaotic motion, it is spread over the entire chaotic layer. If the classical dynamics is mixed, quantum-mechanical states can be classified as regular or chaotic according to their distribution in phase space [62]. Moreover, the phase-space representation of the asymptotic state of a dissipative quantum map exhibits the structures of the corresponding classical attractor [23]. However, these analogies find their limit in the Heisenberg uncertainty principle. It does not allow for arbitrarily fine phase-space structures and results in smearing on action scales below \hbar .

5.1 Classical attractor

To describe the classical dissipative dynamics of the driven double well, we add an Ohmic friction force $F_\gamma = -\gamma p$ to the conservative equations (4), (5),

$$\dot{x} = \frac{1}{m}p, \quad (59)$$

$$\dot{p} = -\gamma p - \frac{\partial V(x, t)}{\partial x}. \quad (60)$$

Friction destroys the time-reversal symmetry (21) of the conservative system. Accordingly, dissipation breaks the reflection symmetry of the phase-space portrait with respect to the x -axis, found at zero phase of the driving (cf. Fig. 6).

A constituent feature of dissipative flows is the net exponential contraction of phase-space volume. Therefore, the dynamics is asymptotically confined to an attractor, a measure-zero manifold in phase space to which all trajectories starting from within the surrounding basin of attraction converge. For periodically driven dissipative systems, the attractor is in general also time-dependent with the period of the driving and is adequately described by a stroboscopic map [63–65].

Depending on the parameters that control the dissipative flow, an attractor can consist of fixed points, limit cycles, or manifolds of fractal dimension, less than that of phase space. An adequate concept to characterize the geometry of an attractor is the Hausdorff dimension d_H defined, for example, in Ref. [3]. It typically increases with decreasing contraction rate, so that strange attractors are expected to occur in the regime of weak dissipation of a system that in absence of friction, is chaotic.

The Hausdorff dimension of the classical attractor for the driven double well with dissipation, Eqs. (59), (60), at the parameter values $F = 0.09$ and $\Omega = 0.9\omega_0$, is shown in Fig. 17 for various values of the friction γ . Although the

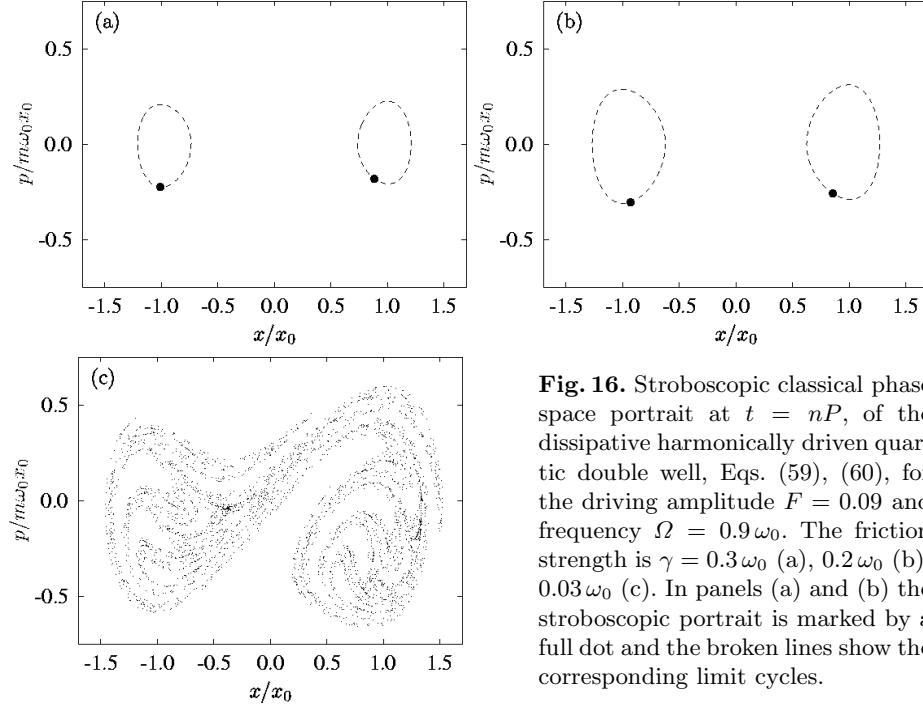


Fig. 16. Stroboscopic classical phase space portrait at $t = nP$, of the dissipative harmonically driven quartic double well, Eqs. (59), (60), for the driving amplitude $F = 0.09$ and frequency $\Omega = 0.9\omega_0$. The friction strength is $\gamma = 0.3\omega_0$ (a), $0.2\omega_0$ (b), $0.03\omega_0$ (c). In panels (a) and (b) the stroboscopic portrait is marked by a full dot and the broken lines show the corresponding limit cycles.

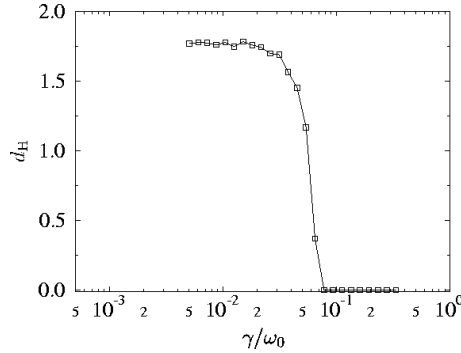


Fig. 17. Hausdorff dimension of the classical attractor of the dissipative harmonically driven quartic double well, Eqs. (59), (60), for $F = 0.09$, $\Omega = 0.9\omega_0$.

attractor itself is periodically time dependent with the period of the driving, its Hausdorff dimension d_H remains nearly constant [63]. Near $\gamma \approx 0.06\omega_0$, with decreasing γ , the classical dynamics undergoes a transition from regular motion to chaos, manifest in a corresponding transition from limit cycles (Fig. 16a,b) to a strange attractor (Fig. 16c) and a concomitant jump in d_H . At the same values of F and Ω , the regular islands near the potential minima of the corresponding undamped dynamics have already completely dissolved in the chaotic sea.

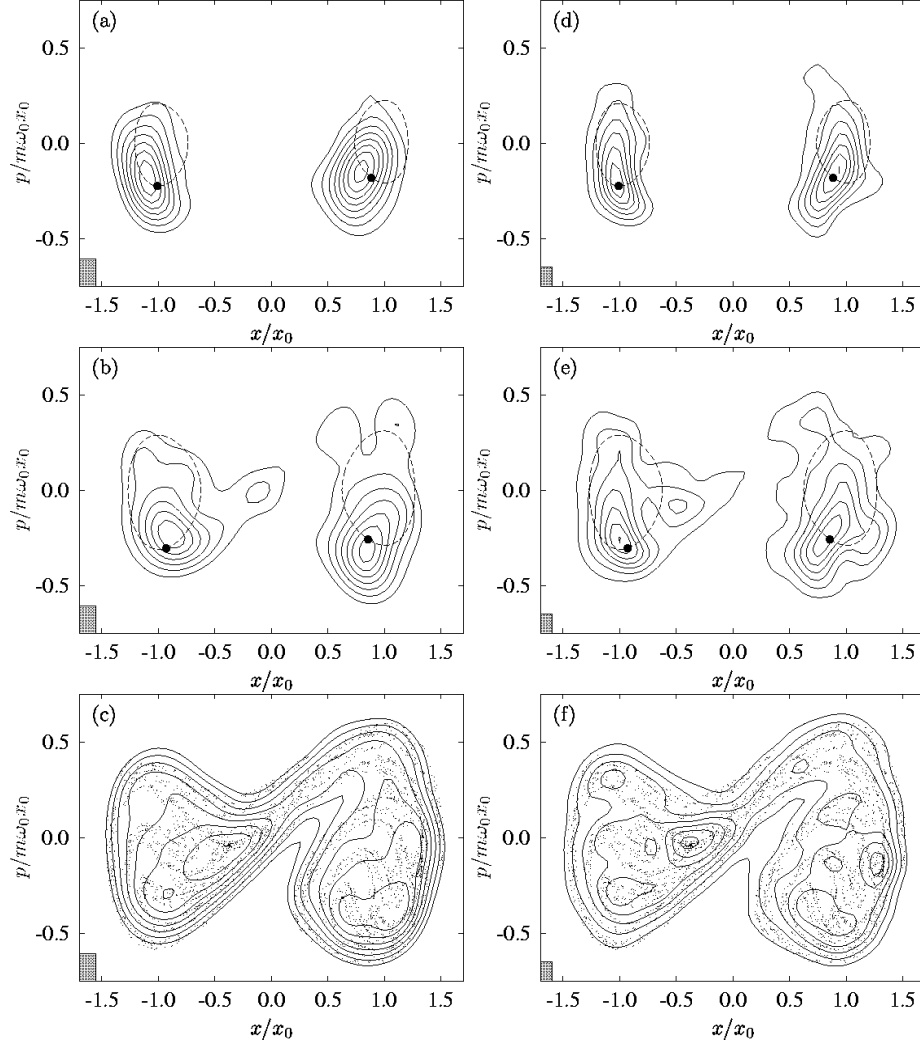


Fig. 18. Contour plot of the Husimi function of the quantum attractor (full lines) at $t = nP$, $n \rightarrow \infty$, superposed on the corresponding classical phase-space portrait, Fig. 16. The parameter values $F = 0.09$, $\Omega = 0.9\omega_0$, $\gamma = 0.3\omega_0$ (a,d), $0.2\omega_0$ (b,e), $0.03\omega_0$ (c,f) are as in Fig. 16. The effective action is $D = 6$ (a–c) and $D = 12$ (d–f). The rectangle in the lower left corner has the size of the effective quantum of action $\hbar_{\text{eff}} = 1/8D$.

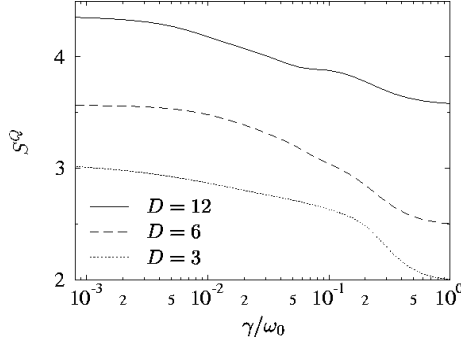


Fig. 19. Wehrl entropy of the asymptotic state of the dissipative quantum map for different values of the effective quantum of action $\hbar_{\text{eff}} = 1/8D$. Other parameters as in Fig. 17.

5.2 Quantum attractor

The “quantum attractors”, i.e., the asymptotic states of the dissipative quantum dynamics, for example in a Husimi representation, resemble the corresponding classical attractors up to coarse graining (Fig. 18). Correspondingly, the qualitative transformation from limit cycles to a strange attractor is visible in the asymptotic quantum distribution, but proceeds continuously. Although the asymptotic state for $\gamma = 0.2\omega_0$ (Fig. 18b,e), is still concentrated near the fixed points of the classical stroboscopic map, it covers a broader phase-space area that already anticipates the shape of the strange attractor. Reducing the effective quantum of action $\hbar_{\text{eff}} = 1/8D$ allows for a sharper resolution of the underlying classical structures in the Husimi functions, as expected.

Like the attractors of the dissipative classical dynamics (Fig. 16), their quantum-mechanical counterparts have lost the reflection symmetry with respect to the x -axis, in contrast to the Husimi representations of the Floquet states in absence of dissipation (cf. Fig. 7). This symmetry breaking is caused by finite off-diagonal elements of the asymptotic density matrix in Floquet representation, since diagonal representations share the symmetries of the basis. Thus, off-diagonal matrix elements play a significant rôle for the asymptotic state. This demonstrates that a description within a full rotating-wave approximation is insufficient, since it would result in an asymptotic state diagonal in the Floquet representation [51–53].

Because the quantum attractor, in contrast to the classical one, has support all over phase space (or a region of finite measure), we cannot characterize it by a Hausdorff dimension. A more suitable measure for the extension of the quantum attractor is a phase-space version of the Shannon entropy, the Wehrl entropy [62, 66, 67]

$$S^Q = - \int \frac{dx dp}{2\pi\hbar} Q(x, p) \ln[Q(x, p)] \quad (61)$$

of its Husimi representation

$$Q(x, p) = \langle x, p | \rho_S | x, p \rangle, \quad (62)$$

where $|x, p\rangle$ denotes a coherent state centered at (x, p) in phase space. Its exponential, $\exp(S^Q)$, gives approximately the number of coherent states covered by the Husimi function. Thus, the occupied phase-space area is $2\pi\hbar \exp(S^Q)$. The Wehrl entropy of the asymptotic state for our numerical example is depicted in Fig. 19 for various values of $\hbar_{\text{eff}} = 1/8D$. It grows with decreasing friction γ , reflecting the increasing dispersion of the Husimi functions. In the semiclassical regime, i.e., for a sufficiently large value of the effective action D , we observe a kink-like behavior of the entropy near $\gamma \approx 0.06 \omega_0$, where the classical attractor undergoes the transition mentioned above, from a set of isolated fixed points to a strange attractor.

Note that for $\gamma \gtrsim 0.1 \omega_0$, the Markov approximation becomes inaccurate, since γ is then of the order of the mean level spacing and the condition (43) is violated for at least part of the transitions between Floquet states. Nevertheless, we obtain the qualitative behavior which we expected from classical considerations.

6 Conclusion

For the generic situation of the dissipative quantum dynamics of a particle in a driven double-well potential, classical chaos plays a significant rôle for the coherent dynamics. Even for arbitrarily small driving amplitude, the separatrix is replaced by a chaotic layer, while the motion near the bottom of the wells remains regular. Nevertheless, the influence of states located in the chaotic region alters the splittings of the regular doublets and thus the tunnel rates, which is the essence of chaotic tunneling. We have studied chaotic tunneling in the vicinity of crossings of chaotic singlets with tunnel doublets under the influence of an environment. As a simple intuitive model to compare against, we have constructed a three-state system which in the case of vanishing dissipation, provides a faithful description of an isolated singlet-doublet crossing. Dissipation introduces new time scales to the system: one for the loss of coherence and a second one for the relaxation to an asymptotic state. Well outside the crossing, both time-scales are of the same order, reflecting an effective two-state behavior. The center of the crossing is characterized by a strong mixing of the chaotic state with one state of the tunnel doublet. The high mean energy of the chaotic state introduces additional decay channels to states outside the three-state system. Thus, decoherence becomes far more effective and, accordingly, tunneling fades out much faster.

The study of the asymptotic state, the quantum attractor, demonstrates clearly that a three-state model of the singlet-doublet crossing is insufficient once dissipation is effective. This is so because the coupling to the heat bath enables processes of decay and thermal activation that connect the states in the crossing with other, “external” states of the central system. In the presence of driving, the asymptotic state is no longer literally a state of equilibrium. Rather, incoherent processes create a steady flow of probability involving states within

as well as outside the crossing. As a result, the composition of the asymptotic state, expressed for example by its coherence $\text{tr} \rho_{\infty}^2$, is markedly different at the center of the crossing as compared to the asymptotic state far away from the crossing, even if that is barely visible in the corresponding classical phase-space structure.

With increasing driving amplitude, in absence of dissipation, even the dynamics near the bottom of the wells becomes fully chaotic. This has striking consequences for the corresponding dissipative classical dynamics: For sufficiently weak dissipation, it remains chaotic, but for strong friction it becomes regular. Accordingly, the geometry of the classical attractor is fractal or regular, respectively. We have observed the signatures of this qualitative difference in the asymptotic state of the corresponding quantum dynamics. However, in contrast to the sudden change of the classical behavior, the quantum attractor undergoes a smooth transition: The structure of the strange attractor is already felt by the Husimi function for parameter values where the classical attractor consists only of two isolated fixed points. For the observation of these semiclassical structures, off-diagonal matrix elements of the asymptotic state in Floquet basis proved crucial. This clearly indicates that a full rotating-wave approximation must fail.

Many more phenomena at the overlap of chaos, tunneling, and dissipation await being unraveled. They include four-state crossings formed when two doublets intersect, chaotic Bloch tunneling along extended potentials with a large number of unit cells instead of just two, and the influence of decoherence on a multi-step mechanism of chaotic tunneling. These phenomena are typically observed in the far semiclassical regime, which requires to take very many levels into account. A semiclassical description of the dissipative quantum system may circumvent this problem.

References

- [1] G. Casati, B. V. Chirikov, F. M. Izrailev, and J. Ford, in *Stochastic Behavior in Classical and Quantum Hamiltonian Systems*, Vol. 93 of *Lecture Notes in Physics*, edited by G. Casati and J. Ford (Springer, Berlin, 1979), p. 334.
- [2] T. Dittrich and R. Graham, *Ann. Phys. (N.Y.)* **200**, 363 (1990).
- [3] E. Ott, *Chaos in Dynamical Systems*, Cambridge University Press (Cambridge 1993).
- [4] M.J. Davis and E.J. Heller, *J. Chem. Phys.* **75**, 246 (1981).
- [5] O. Bohigas, S. Tomsovic, and D. Ullmo, *Phys. Rev. Lett.* **64**, 1479 (1990).
- [6] O. Bohigas, S. Tomsovic, and D. Ullmo, *Phys. Rev. Lett.* **65**, 5 (1990).
- [7] O. Bohigas, S. Tomsovic, and D. Ullmo, *Phys. Rep.* **223**, 43 (1993).
- [8] S. Tomsovic and D. Ullmo, *Phys. Rev. E* **50**, 145 (1994).
- [9] W. A. Lin and L. E. Ballentine, *Phys. Rev. Lett.* **65**, 2927 (1990).
- [10] W. A. Lin and L. E. Ballentine, *Phys. Rev. A* **45**, 3637 (1992).
- [11] R. Utermann, T. Dittrich, and P. Hänggi, *Phys. Rev. E* **49**, 273 (1994).
- [12] P. Hänggi, R. Utermann, and T. Dittrich, *Physica B* **194-196**, 1013 (1994).
- [13] M. Latka, P. Grigolini, and B. J. West, *Phys. Rev. E* **50**, 596 (1994).

- [14] M. Latka, P. Grigolini, and B. J. West, Phys. Rev. A **50**, 1071 (1994).
- [15] M. Latka, P. Grigolini, and B. J. West, Phys. Rev. E **50**, R3299 (1994).
- [16] E. M. Zanardi, J. Gutiérrez, and J. M. Gomez Llorente, Phys. Rev. E **52**, 4736 (1995).
- [17] E. Doron and S. D. Frischat, Phys. Rev. Lett **75**, 3661 (1995).
- [18] S. D. Frischat and E. Doron, Phys. Rev. E **57**, 1421 (1998).
- [19] F. Leyvraz and D. Ullmo, J. Phys. A **29**, 2529 (1996).
- [20] R. Roncaglia, L. Bonci, F. M. Izrailev, B. J. West, and P. Grigolini, Phys. Rev. Lett. **73**, 802 (1994).
- [21] A. O. Caldeira and A. L. Leggett, Ann. Phys. (N.Y.) **149**, 374 (1983); erratum: Ann. Phys. (N.Y.) **153**, 445 (1984).
- [22] M. Grifoni and P. Hänggi, Phys. Rep. **304**, 219 (1998).
- [23] T. Dittrich and R. Graham, Europhys. Lett. **4**, 263 (1987).
- [24] J. H. Shirley, Phys. Rev. **138**, B979 (1965).
- [25] H. Sambe, Phys. Rev. A **7**, 2203 (1973).
- [26] N. L. Manakov, V. D. Ovsiannikov, and L. P. Rapoport, Phys. Rep. **141**, 319 (1986).
- [27] S.-I. Chu, Adv. Chem. Phys. **73**, 739 (1989).
- [28] T. Dittrich, P. Hänggi, G.-L. Ingold, B. Kramer, G. Schön, and W. Zwerger, *Quantum Transport and Dissipation* (Wiley-VCH, Weinheim, 1998).
- [29] D. J. Moore, Helv. Phys. Acta **66**, 3 (1993).
- [30] M. L. Mehta, *Random matrices and the statistical theory of energy levels* (Academic Press, New York, 1967).
- [31] F. Haake, *Quantum Signatures of Chaos*, Vol. 54 of *Springer Series in Synergetics* (Springer, Berlin, 1991).
- [32] F. Grossmann, T. Dittrich, P. Jung, and P. Hänggi, Phys. Rev. Lett. **67**, 516 (1991).
- [33] F. Grossmann, P. Jung, T. Dittrich, and P. Hänggi, Z. Phys. B **84**, 315 (1991).
- [34] A. Peres, Phys. Rev. Lett. **67**, 158 (1991).
- [35] F. Grossmann and P. Hänggi, Europhys. Lett. **18**, 571 (1992).
- [36] P. Hänggi, P. Talkner, and M. Borkovec, Rev. Mod. Phys. **62**, 251 (1990).
- [37] T. Dittrich, B. Oelschlägel, and P. Hänggi, Europhys. Lett. **22**, 5 (1993).
- [38] B. Oelschlägel, T. Dittrich, and P. Hänggi, Acta Physica Polonica B **24**, 845 (1993).
- [39] T. Dittrich, P. Hänggi, B. Oelschlägel, and R. Utermann, in *25 Years of Non-Equilibrium Statistical Mechanics*, Vol. 445 of *Lecture Notes in Physics*, edited by J. J. Brey (Springer, Berlin, 1995), p. 269.
- [40] A. J. Lichtenberg and M. A. Liebermann, *Regular and Stochastic Motion*, Vol. 38 of *Applied Mathematical Sciences* (Springer, New York, 1983).
- [41] D. F. Escande, Phys. Rep. **121**, 165 (1985).
- [42] L. E. Reichl and W. M. Zheng, in *Directions in Chaos*, edited by H. B. Lin (World Scientific, Singapore, 1987), Vol. 1, p. 17.
- [43] M. Wilkinson, Physica D **21**, 341 (1986).
- [44] M. Wilkinson, J. Phys. A **20**, 635 (1987).
- [45] S. Kohler, R. Utermann, P. Hänggi, and T. Dittrich, Phys. Rev. E **58**, 7219 (1998).
- [46] L. E. Reichl, *The Transition to Chaos: In Conservative and Classical Systems: Quantum Manifestations* (Springer, New York, 1992).
- [47] R. B. Shirts and W. P. Reinhardt, J. Chem. Phys. **77**, 5204 (1982).

- [48] A first quantum Langevin formulation has been given by: V. B. Magalinskii, *Zh. Eksp. Teor. Fiz.* **36**, 1942 (1959), [*Sov. Phys. JETP* **9**, 1381 (1959)].
- [49] Classical formulations of the system-harmonic oscillator bath coupling scheme have been put forward by: N. N. Bogoliubov, in *On some statistical methods in mathematical physics* (Ukr. S.S.R. Acad. of Science Press, 1945), p. 115 (in russian); R. Zwanzig, *J. Stat. Phys.* **9**, 215 (1973).
- [50] F. Haake, in *Quantum Statistics in Optics and Solid-State Physics*, Vol. 66 of *Springer Tracts in Modern Physics*, edited by G. Höhler (Springer, Berlin, 1973).
- [51] R. Blümel *et al.*, *Phys. Rev. Lett.* **62**, 341 (1989).
- [52] R. Blümel *et al.*, *Phys. Rev. A* **44**, 4521 (1991).
- [53] R. Graham and R. Hübner, *Ann. Phys. (N.Y.)* **234**, 300 (1994).
- [54] S. Kohler, T. Dittrich, and P. Hänggi, *Phys. Rev. E* **55**, 300 (1997).
- [55] D. E. Makarov and N. Makri, *Phys. Rev. E* **52**, 5863 (1995).
- [56] N. Makri, *J. Chem. Phys.* **106**, 2286 (1997).
- [57] T. Dittrich and U. Smilansky, *Nonlinearity* **4**, 59 (1991).
- [58] K. Takahashi and N. Saitô, *Phys. Rev. Lett.* **55**, 645 (1985).
- [59] S.-J. Chang and K.-J. Shi, *Phys. Rev. Lett.* **55**, 269 (1985).
- [60] S.-J. Chang and K.-J. Shi, *Phys. Rev. A* **34**, 7 (1986).
- [61] B. Mirbach and H. J. Korsch, *J. Phys. A* **27**, 6579 (1994).
- [62] T. Gorin, H. J. Korsch, and B. Mirbach, *Chem. Phys.* **217**, 145 (1997).
- [63] F. C. Moon and G.-X. Li, *Physica D* **17**, 99 (1985).
- [64] F. C. Moon and G.-X. Li, *Phys. Rev. Lett.* **55**, 1439 (1985).
- [65] W. Szemplinska-Stupnicka, *Nonlinear Dynamics* **3**, 225 (1992).
- [66] A. Anderson and J. J. Halliwell, *Phys. Rev. D* **48**, 2753 (1993).
- [67] A. Wehrl, *Reps. Math. Phys.* **16**, 353 (1979); *Reps. Math. Phys.* **30**, 119 (1991).